Pt-Nanoparticles on ZnO/Carbon Quantum Dots: A Trifunctional Nanocomposite with Superior Electrocatalytic Activity Bosting Direct Methanol Fuel Cell and Zinc-Air Battery

Anup Kumar Pradhan,[a] Sayan Halder,[a] and Chanchal Chakraborty*[,a,b]

[a] Department of Chemistry, Birla Institute of Technology & Science (BITS) Pilani, Hyderabad Campus. Jawaharnagar, Samirpet, Hyderabad, Telangana 500078, India.

[b] Materials Center for Sustainable Energy & Environment (McSEE), Birla Institute of Technology and Science, Hyderabad Campus, Hyderabad 500078, India

*Corresponding Author: Chanchal Chakraborty

E-mail: chanchal@hyderabad.bits-pilani.ac.in

Rotating disk electrode (RDE) measurements:

In RDE measurements, electrode materials were cathodically scanned from 0.2 to -0.8 V (vs. SCE) in 0.1M KOH at a scan rate of 10 mV s^{-1} with different rotation speeds from 400 to 3000 rpm. Koutecky-Levich plots are derived from CLSV data measured from the RDE experiment and calculate the electron transferred number based on the following K-L equation,

$$\frac{1}{j} = \frac{1}{jl} + \frac{1}{jk} = \frac{1}{B\omega^{1/2}} + \frac{1}{jk}$$

$B = 0.2nFC_0(D_0)^{2/3}\, v^{-1/6}$

Where, j = current density

j_l & j_k = diffusion- and kinetic-limiting current densities

ω = angular velocity

F = Faraday constant

C_0 = bulk concentration of O_2

D_0 = diffusion coefficient of O_2 in electrolyte

N = number of electrons transferred

v = kinematic viscosity of the electrolyte.

Rotating ring-disk electrode (RRDE) measurements:

In RRDE measurements, electrode material was cathodically scanned from 0.2 to -0.8 V (vs. SCE) at the scan rate of 10 mV s-1 in 0.1M KOH, keeping ring potential constant at 1.5 V vs. RHE. The number of electrons transferred (n) and peroxide yield (%) were calculated by using the following equations,

$$H_2O_2\ (\%) = 200 \times \frac{I_r/N}{I_d + I_r/N}$$

$$n = 4 \times \frac{I_d}{I_d + I_r/N}$$

Where, I_d = disk current

I_r = ring current

N = current collection efficiency of the Pt ring (37%)

Calculation of the Battery Performances:

The specific capacity of the assembled zinc-air batteries was calculated from the equation below:

$$Specific\ capacity = I \times t/m_{Zn}$$

The energy can be calculated from the equation below:

$$Energy\ density = I \times t \times V/m_{Zn}$$

Where I denotes current, t denotes the service hours, V denotes the average discharge voltage, and m_{Zn} denotes the weight of consumed zinc.

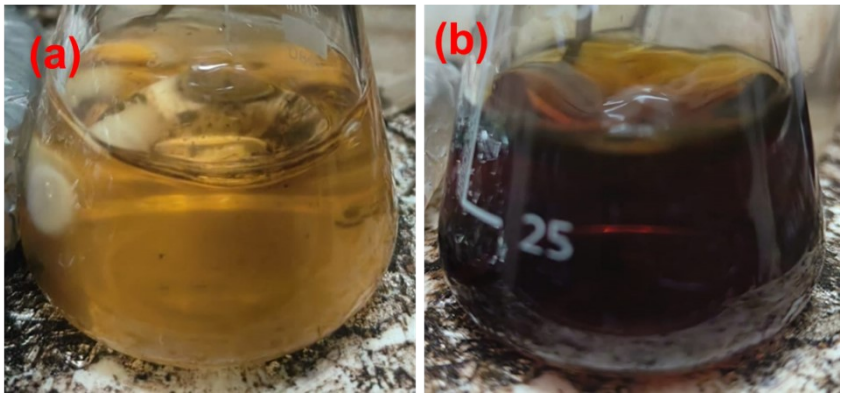

Fig. S1. The color change of the reaction mixture (a) before and (b) after adding the Pt precursor to synthesize PtNP-ZnO@CQDs.

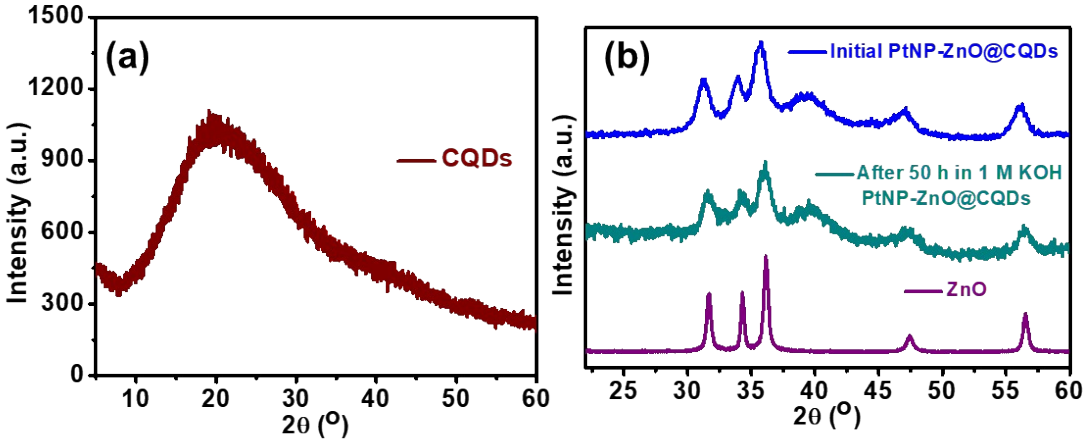

Fig. S2 (a) The PXRD pattern of CQDs. (b) (b) The comparison of the XRD pattern of ZnO, pristine PtNP-ZnO@CQDs, and PtNP-ZnO@CQDs after soaking in 1 M KOH for 50 h.

Table. S1. BET isotherm data of Pt-ZnO/CQDs nanocomposite

Parameter	**Values**
Specific surface area (m^2/g)	81.565 m^2/g
Mean pore diameter (nm)	6.9365 nm
Total pore volume (cm^3/g)	0.2029 cm^3/g

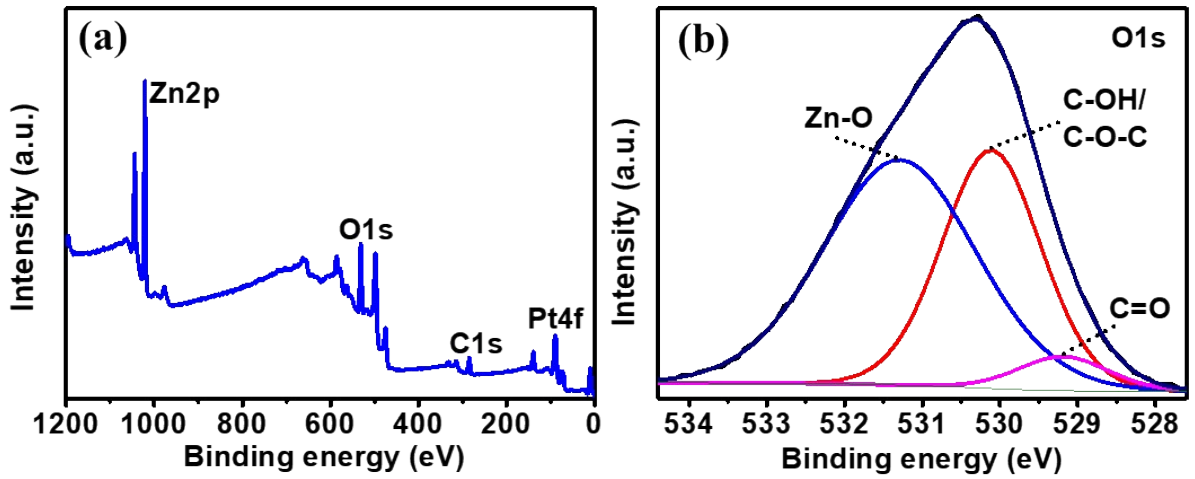

Fig. S3 (a) Survey spectra of Pt-ZnO/CQDs nanocomposite and **(b)** O1s spectra of Pt-ZnO/CQDs nanocomposite.

Table S2: Elemental analysis with weight and atomic percentages of different elements from the EDX study

Element	Line Type	Apparent Concentration	k Ratio	Wt%	Wt% Sigma	Atomic %
C	K series	146.92	1.4692	69.23	0.10	86.94
O	K series	22.72	0.07652	9.15	0.08	8.63
Zn	K series	80.82	0.80610	17.97	0.08	4.14
Pt	M series	15.89	0.15894	3.65	0.04	0.29
Total:				100.00		100.00

Table S3: The comparison of elemental analysis using XPS, EDX, and AAS studies.

Elements	Wt% by XPS	Wt% by EDX	Wt% by AAS
Pt	3.16	3.65	4.75
Zn	15.8	17.97	19.22

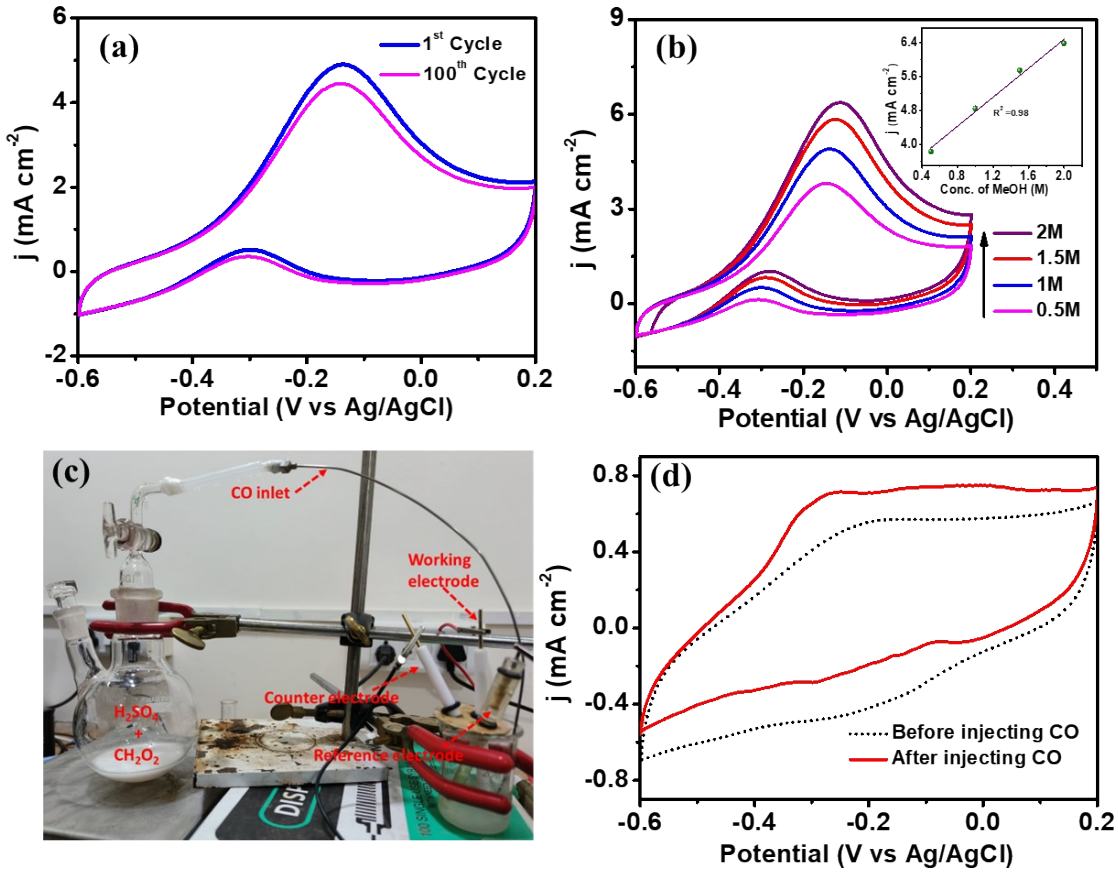

Fig. S4 (a) Cycle stability performance of **PtNP-ZnO@CQDs** nanocomposite electrocatalyst. (b) CV of different molar concentrations of methanol into 1M of KOH electrolyte solution. (c) Laboratory setup for CO striping experiment. (d) CV of CO striping on **PtNP-ZnO@CQDs** modified glassy carbon electrode.

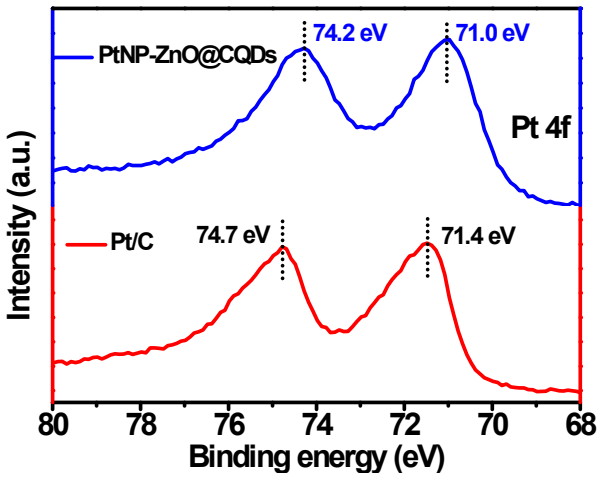

Fig. S5 Core level XPS spectra of Pt4f in PtNP-ZnO@CQDs and comparison with commercial Pt/C.

Table S4. Comparison of electrocatalytic OER activity of PtNP-ZnO@CQDs with recently reported catalysts.

Electrocatalysts	**Synthesis method**	**Electrolyte KOH (M)**	**Overpotential (mV) @ 10 mA/cm²**	**Tafel slope (mV/dec)**	**Ref.**
$ZnCo_2O_4$ nanosheets with oxygen vacancies	Hydrothermal and $NaBH_4$ reduction	0.1	324	56.9	1
V-Co-Fe-343	hydrothermal	1.0	307	36.0	2
$SmBa_{0.5}Sr_{0.5}Co_2O_{6-\delta}$ (SBSC-E(800))	hydrothermal	0.1	370	46.0	3
ZnO@NiFe core-shell nanorods	electrodeposition	0.1	380	105	4
$Co_{0.54}Fe_{0.46}(OOH)$	electrodeposition	1.0	370	26	5
Au/NiFe LDH	hydrothermal	1.0	237	36	6
(Co,Ni)Se2@NiFe-LDH	solvothermal	1.0	332	75	7
Co_2P/Co_4N/CNTs	Pyrolysis	1.0	389	110	8
PtNP-ZnO@CQDs	**one-pot hydrothermal**	**1.0**	**355**	**61.7**	**This Work**

Calculation of Faradic Efficiency:

The chronoamperometry study of Pt-ZnO/CQDs was conducted at a voltage of 1.6 V (RHE) for 30 min (in **Fig. S6a**). Therefore,

The charge passed (area under the curve) = 36.246 Coulomb

Again, 36.246 Coulomb = (36.246/96485) mole electron

Here, one oxygen molecule was evolved by 4 electrons pathway, so the theoretical oxygen production = (36.246/(96485×4)) mole

= (36.246×22400)/(96485×4) mL (1 mole gas = 22400 mL at STP)

= 2.10 mL

Using the water displacement method, the amount of oxygen evolved was collected and measured in a centrifuge tube (in **Fig. S6b**). The Faradic Efficiency (FE) at 1.6 V (RHE) was calculated using the following equation.

FE = (amount of O_2 evolved (mL) × 100) / Theoretical yield of O_2 (mL)

FE = (1.95× 100)/2.10

FE = 93 %

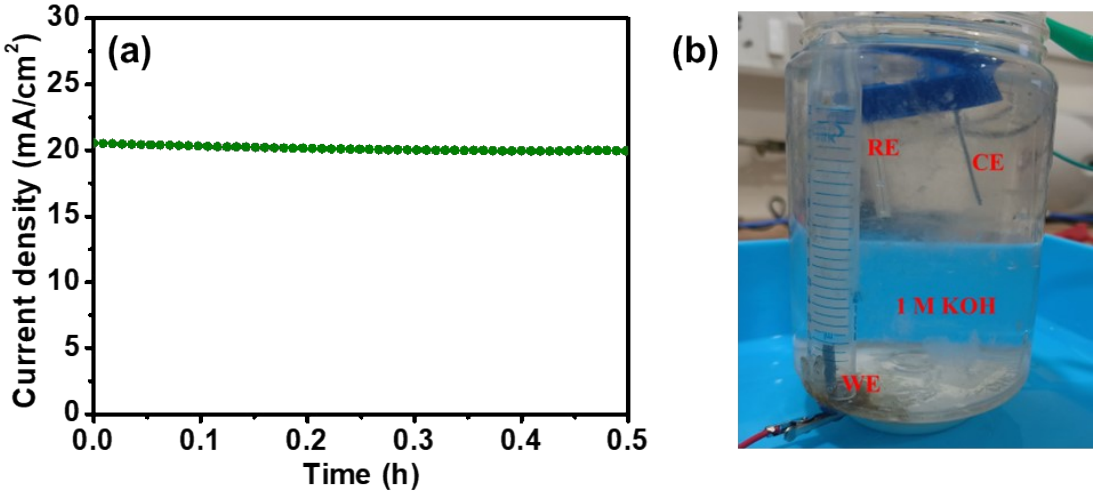

Fig. S6. (a) The chronoamperometry plot. (b) Set-up for measuring the evolved oxygen by self-made instrument and the amount of oxygen evolved after 30 min during chronoamperometry.

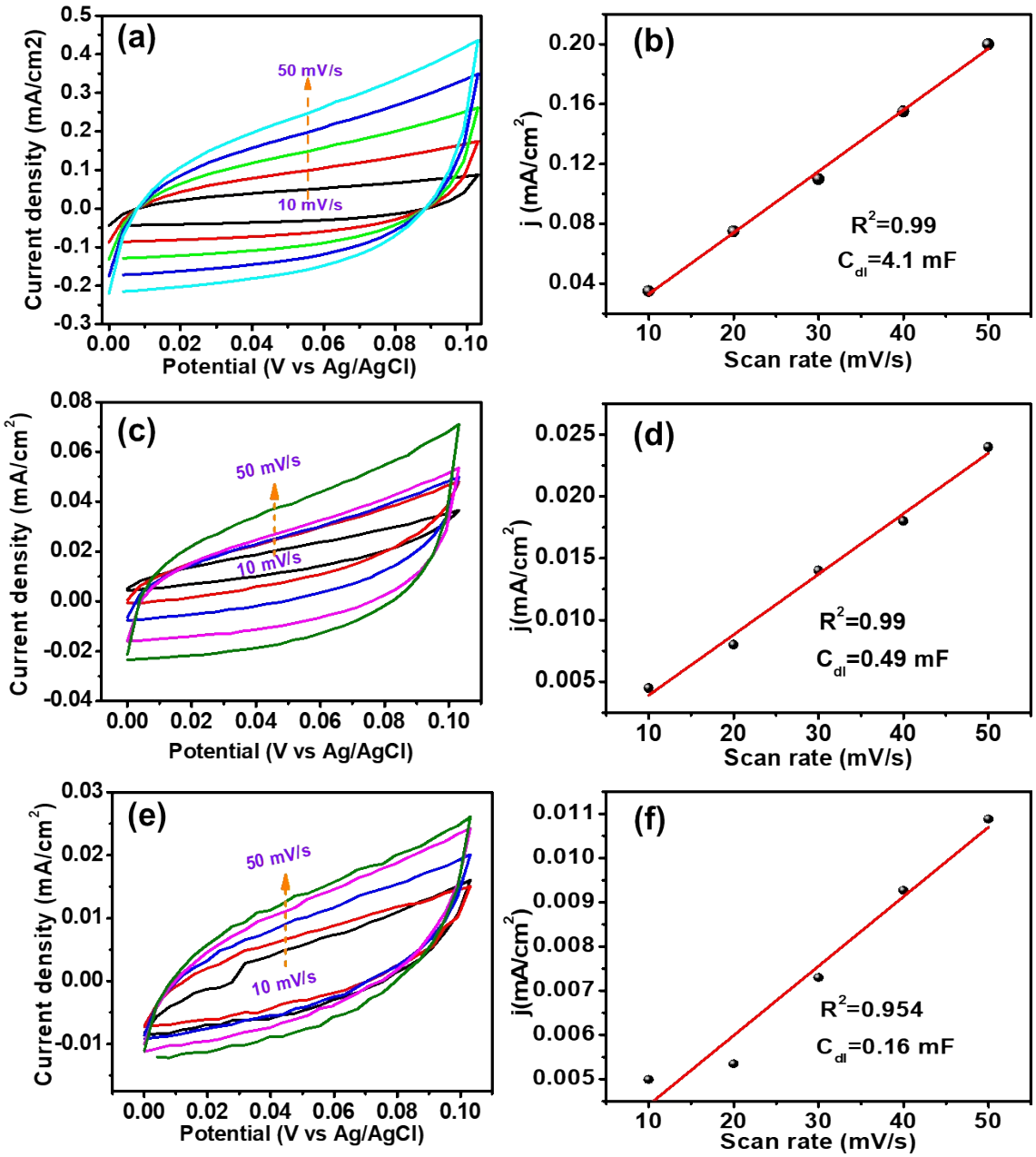

Fig. S7. The CV curves were obtained in the non-Faradic region and corresponding C_{dl} calculation for (a-b) PtNP-ZnO@CQDs, (c-d) ZnO, and (e-f) CQDs at different scan rates from 10 to 50 mV/s.

Table S5. Compared values of ECSA and R_{CT} for PtNP-ZnO@CQDs with the intermediate ZnO and CQDs.

Catalysts	C_{dl} (mF)	ECSA (cm^2)	R_{CT} (Ω)
PtNP-ZnO@CQDs	4.1	68.3	23.1
ZnO	0.49	8.2	28.7
CQDs	0.16	2.6	34.3

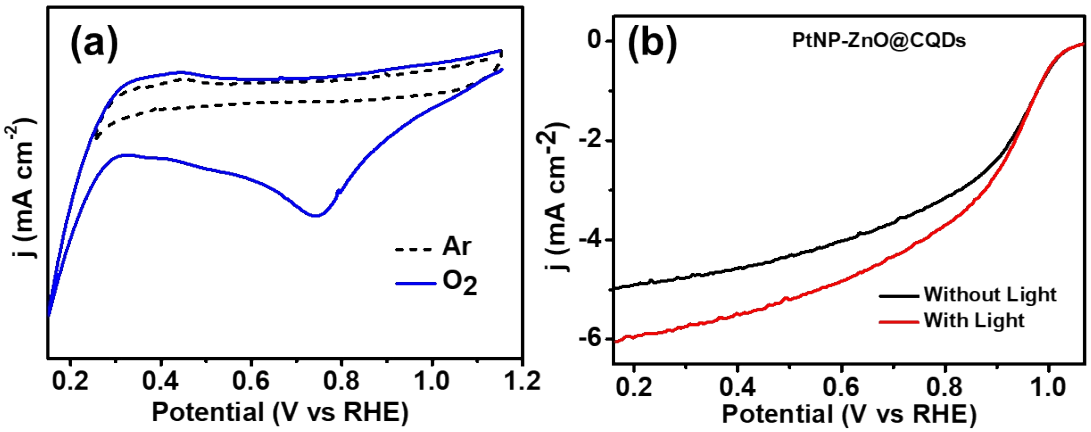

Fig. S8 (a) CV study for oxygen reduction for PtNP-ZnO@CQDs catalyst. No reduction was shown in argon-saturated electrolytes. **(b)** CLSV plot of PtNP-ZnO@CQDs during ORR in the presence and absence of light irradiation.

Table S6. Comparison of electrocatalytic ORR activity of PtNP-ZnO@CQDs with recently reported Pt-based catalysts.

Electrocatalysts	**Synthesis method**	**Pt-content (wt%)**	**Limiting current density (mA cm^{-1})**	**Mass Activity A (A mg_{pt}^{-1})**	**$E_{1/2}$ (V)**	**Reference**
Pt&CoO/N-doped carbon (NC)	2 steps pyrolysis	~2	~5.3	-	0.842	9
Pt&Fe_2O_3/N-doped carbon (NC)	2 steps pyrolysis	~2	~5.4	-	0.862	9
Pt/Ta/SnO_2	Microwave	7	~5.5	0.465	~0.9	10
Pt/$TiNbO_x$ (Ti/Nb = 1:6.6)/CSCNT	Photo-deposition	~20	~5.8	1.06	~0.9	11
PtNi/Mn_2O_3-NiO	Microwave	8.68	4.32	-	~0.8	12
PtNi/Mn_2O_3-TiO_2	Microwave	8.23	2.02	-	~0.7	12
PtNi hollow nanochain	galvanic replacement	77	~5.5	0.34	0.856	13
PtNi nanoporous nanowires	Eutectic reaction	78.74	~6	0.333	0.898	14
PtZn intermetallic nanocrystals	Atomic layer deposition	66.1	~6.1	0.27	0.887	15
Pt_3Co/Co_3ZnC@Co-N-doped Carbon	two-step pyrolysis	11.95	~5.1	0.156	0.9	16
PtFe nanowires	Electrochemical etching	~20	~6	1.10	0.959	17
1 nm PtFeCo nanowire	solvothermal	~20	~5.5	0.57	~0.85	18
Pt_xCo_{1-x} core–shell catalysts	Impregnation and annealing	-	~6	0.15	0.95	19
Pt_2Pd porous alloy	molten-alkali mechanochemical	-	~6	1.38	0.9	20
$Pd_{45}Pt_{44}Ni_{11}$ Spiral	one-pot hydrothermal	-	~5.7	1.86	0.94	21
PtNP-ZnO@CQDs	**one-pot hydrothermal**	**5.4**	**5.0**	**0.426**	**0.95**	**This Work**

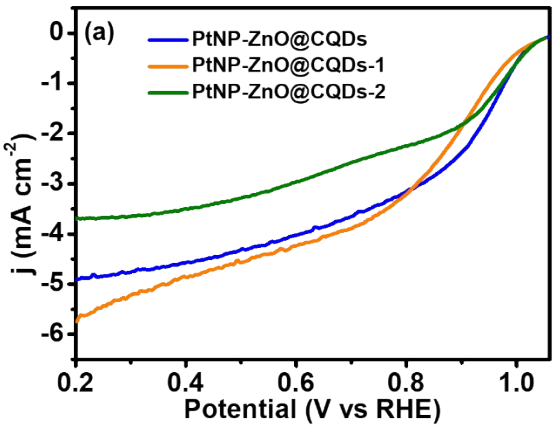

(b)

	Pt (m mol)	Zn (m mol)	Ratio (Pt:Zn)
PtNP-ZnO@CQDs	0.244	125	0.001952:1
PtNP-ZnO@CQDs-1	0.488	125	0.003904:1
PtNP-ZnO@CQDs-2	0.122	125	0.000976:1

Fig. S9 (a) ORR activity of various **PtNP-ZnO@CQDs** catalysts. (b) Summary of the amount of metal present in the catalyst.

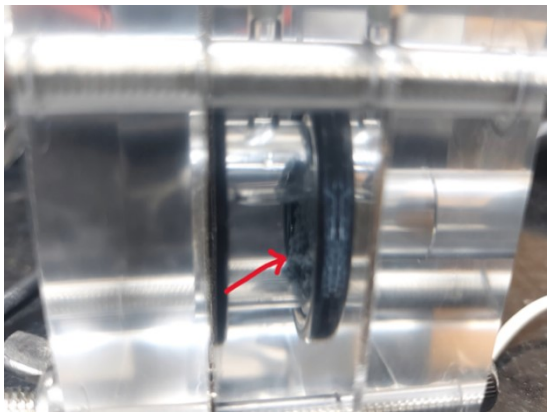

Fig. S10 Image of degradation of zinc plate during ZAB operation.

References

1. K. Xiang, D. Wu, Y. Fan, W. You, D. Zhang, J.-L. Luo, X.-Z. Fu, Enhancing bifunctional electrodes of oxygen vacancy abundant $ZnCo_2O_4$ nanosheets for supercapacitor and oxygen evolution, *Chem. Eng. J.* 425 (2021) 130583, https://doi.org/10.1016/j.cej.2021.130583.

2. T. Gao, Z. Jin, M. Liao, J. Xiao, H. Yuan, D. Xiao, A trimetallic V−Co−Fe oxide nanoparticle as an efficient and stable electrocatalyst for oxygen evolution reaction. *J. Mater. Chem. A* 3 (2015) 17763−17770. DOI: 10.1039/C5TA04058B
3. H. Zhang, D. Guan, X. Gao, J. Yu, G. Chen, W. Zhou, Z. Shao, Morphology, crystal structure and electronic state one-step co-tuning strategy towards developing superior perovskite electrocatalysts for water oxidation, *J. Mater. Chem. A*, 7 (2019) 19228-19233. https://doi.org/10.1039/C9TA06020K
4. Z. Zhao, H. Wu, H. He, X. Xu, Y. Jin, Self-standing non-noble metal (Ni−Fe) oxide nanotube array anode catalysts with synergistic reactivity for high-performance water oxidation. *J. Mater. Chem. A* 3 (2015) 7179−7186. DOI: 10.1039/C5TA00160A
5. M.-S. Burke, M.-G. Kast, L. Trotochaud, A.-M. Smith, S.-W. Boettcher, Cobalt-iron (oxy)hydroxide oxygen evolution electrocatalysts: the role of structure and composition on activity, stability, and mechanism. *J. Am. Chem. Soc.* 137 (2015) 3638−3648. DOI: 10.1021/jacs.5b00281
6. J. Zhang, J. Liu, L. Xi, Y. Yu, N. Chen, S. Sun, W. Wang, K.-M. Lange, B. Zhang, Single-atom Au/NiFe layered double hydroxide electrocatalyst: probing the origin of activity for oxygen evolution reaction. *J. Am. Chem. Soc.* 140 (2018) 3876−3879. DOI: 10.1021/jacs.8b00752
7. J.-G. Li, H. Sun, L. Lv, Z. Li, X. Ao, C. Xu, Y. Li, C. Wang, Metal–organic framework-derived hierarchical (Co, Ni) Se2@ NiFe LDH hollow nanocages for enhanced oxygen evolution. *ACS Appl. Mater. Interfaces* 11 (2019) 8106-8114. DOI: doi.org/10.1021/acsami.8b22133
8. Z. Cai, L. Xu, Y. Zhou, L. Gao, X. An, X. Ma, Y. Ma, J. Liu, X. Li, K. Tang, Fabrication of cobalt phosphide/nitride/carbon nanotube composite: An efficient

bifunctional catalyst for hydrogen and oxygen evolution, International Journal of Hydrogen Energy, 82 (2024) 559-566. https://doi.org/10.1016/j.ijhydene.2024.07.394

9. H.-J. Zhang, Z. Zhou, L. Jia, Z.-F. Ma, Y. Xue, Collaborative Anchoring of Pt Nanoparticles and Metal Oxide Nanoparticles on N-Doped Carbon as Catalysts for Oxygen Reduction, *ACS Appl. Nano Mater.* 6 (2023) 13314-13319. DOI: 10.1021/acsanm.3c02011
10. I. Jiménez-Morales, F. Haidar, S. Cavaliere, D. Jones, J. Rozière, Strong Interaction between Platinum Nanoparticles and Tantalum-Doped Tin Oxide Nanofibers and Its Activation and Stabilization Effects for Oxygen Reduction Reaction, *ACS Catal.* 10 (2020) 10399-10411. DOI: 10.1021/acscatal.0c02220
11. F. Ando, T. Gunji, T. Tanabe, I. Fukano, H. D. Abruña, J. Wu, T. Ohsaka, F. Matsumoto, Enhancement of the Oxygen Reduction Reaction Activity of Pt by Tuning Its d-Band Center via Transition Metal Oxide Support Interactions, *ACS Catal.* 11 (2021) 9317-9332, DOI: 10.1021/acscatal.1c01868
12. D. Mladenović, D. M. F. Santos, G. Bozkurt, G. S. P. Soylu, A. B. Yurtcan, Š. Miljanić, B. Šljukić, Tailoring metal-oxide-supported PtNi as bifunctional catalysts of superior activity and stability for unitized regenerative fuel cell applications, Electrochemistry Communications, 124 (2021) 106963. https://doi.org/10.1016/j.elecom.2021.106963.
13. S. Fu, C. Zhu, J. Song, M.H. Engelhard, Y. He, D. Du, C. Wang, Y. Lin, Three-dimensional PtNi hollow nano chains as an enhanced electrocatalyst for the oxygen reduction reaction, J. Mater. Chem. A 4 (22) (2016) 8755–8761.
14. Y. Wang, K. Yin, L. Lv, T. Kou, C. Zhang, J. Zhang, H. Gao, Z. Zhang, Eutectic directed self-templating synthesis of PtNi nanoporous nanowires with superior

electrocatalytic performance towards the oxygen reduction reaction: experiment and DFT calculation, J. Mater. Chem. A 5 (45) (2017) 23651–23661.

15. C. Huang, H. Liu, Y. Tang, Q. Lu, S. Chu, X. Liu, B. Shan, R. Chen, Constructing uniform sub-3 nm PtZn intermetallic nanocrystals via atomic layer deposition for fuel cell oxygen reduction, Applied Catalysis B: Environmental, 320 (2023) 121986.
16. W. Shi, J. Zhang, X. Dong, J. Chen, G. Wang, R. Wang, Stabilizing Pt_3Co intermetallic nanocrystals on Co_3ZnC/Co in N-doped carbon for efficient oxygen reduction reaction and high-performance zinc-air batteries, Carbon 214 (2023) 118321.
17. Y. Shi, W. Yang, W. Gong, X. Wang, Y. Zhou, X. Shen, Y. Wu, J. Di, D. Zhang, Q. Li, Interconnected surface-vacancy-rich PtFe nanowires for efficient oxygen reduction, J. Mater. Chem. A 9 (21) (2021) 12845–12852.
18. N. Cheng, L. Zhang, Y. Zhou, S. Yu, L. Chen, H. Jiang, C. Li, A general carbon monoxide-assisted strategy for synthesizing one-nanometer-thick Pt-based nanowires as effective electrocatalysts, J. Colloid Interface Sci. 572 (2020) 170–178.
19. P. Weber, D. J. Weber, C. Dosche, M. Oezaslan, Highly Durable Pt-Based Core–Shell Catalysts with Metallic and Oxidized Co Species for Boosting the Oxygen Reduction Reaction, *ACS Catalysis* 12 (2022) 6394-6408, DOI: 10.1021/acscatal.2c00514.
20. Q. Wang, S. Shao, M. Ma, W. Zhu, H. Yang, J. Chen, J. Su, F. Liao, Q. Shao, M. Shao, Flexible Pt_2Pd alloy nanosheet electrocatalysts for efficient oxygen reduction reaction and zinc–air batteries, CrystEngComm, 26 (2024) 1430-1437. DOI: 10.1039/D3CE01211E.
21. K. Liu, H. Huang, Y. Zhu, S. Wang, Z. Lyu, X. Han, Q. Kuang, S. Xie, Edge-segregated ternary Pd–Pt–Ni spiral nanosheets as high-performance bifunctional

oxygen redox electrocatalysts for rechargeable zinc–air batteries, J. Mater. Chem. A 10 (2022) 3808-3817. DOI: 10.1039/D1TA10585J